REPORT DOCUMENTATION PAGE

Form Approved
OMB No. 0704-0188

1. REPORT DATE *(DD-MM-YYYY)*	2. REPORT TYPE	3. DATES COVERED *(From - To)*
04-10-2009	Journal Article	

4. TITLE AND SUBTITLE

Acoustic Observation of the Time Dependence of the Roughness of Sandy Seafloors

5a. CONTRACT NUMBER

5b. GRANT NUMBER

5c. PROGRAM ELEMENT NUMBER

6. AUTHOR(S)

Darrell r. Jackson, Michael d. Richardson, Kevin L. Williams, Anthony P. Lyons, Christopher D. Jones, Kevin B. Briggs, Dajun Tang

5d. PROJECT NUMBER

5e. TASK NUMBER

5f. WORK UNIT NUMBER

7. PERFORMING ORGANIZATION NAME(S) AND ADDRESS(ES)

Naval Research Laboratory
Marine Geoacoustics Division
Stennis Space Center, MS 39529

8. PERFORMING ORGANIZATION REPORT NUMBER

NRL/JA/7430-07-7

9. SPONSORING/MONITORING AGENCY NAME(S) AND ADDRESS(ES)

Office of Naval Research
800 North Quincy Street
Arlington VA 22217-5000

10. SPONSOR/MONITOR'S ACRONYM(S)

ONR

11. SPONSOR/MONITOR'S REPORT NUMBER(S)

12. DISTRIBUTION/AVAILABILITY STATEMENT

Approved for public release; distribution is unlimited

13. SUPPLEMENTARY NOTES

IEEE Journal of Oceanic Engineering, Vol., 34, No. 4, October 2009

14. ABSTRACT

Abstract—**A statistical model for the time evolution of seafloor roughness due to biological activity is applied to photographic and acoustic data. In this model, the function describing small scale seafloor topography obeys a time-evolution equation with a random forcing term that creates roughness and a diffusion term that degrades roughness. When compared to acoustic data from the 1999 and 2004 Sediment Acoustics Experiments (SAX99 and SAX04), the model yields diffusivities in the range from 3.5×10^{-11} to 2.5×10^{-10} $m^2 s^{-1}$ (from 10 to 80 $cm^2 yr^{-1}$), with the larger values occurring at sites where bottom-feeding fish were active. While the experimental results lend support to the model,**

15. SUBJECT TERMS

Acoustic scattering, bioturbation, diffusion processes, seafloor, sediment transport

16. SECURITY CLASSIFICATION OF:			17. LIMITATION OF ABSTRACT	18. NUMBER OF PAGES	19a. NAME OF RESPONSIBLE PERSON
a. REPORT	b. ABSTRACT	c. THIS PAGE			Michael Richardson
Unclassified	Unclassified	Unclassified	UU	16	19b. TELEPHONE NUMBER *(Include area code)* 228-688-4621

Acoustic Observation of the Time Dependence of the Roughness of Sandy Seafloors

Darrell R. Jackson, Michael D. Richardson, Kevin L. Williams, Anthony P. Lyons, *Member, IEEE*, Christopher D. Jones, Kevin B. Briggs, and Dajun Tang

***Abstract*—A statistical model for the time evolution of seafloor roughness due to biological activity is applied to photographic and acoustic data. In this model, the function describing small scale seafloor topography obeys a time-evolution equation with a random forcing term that creates roughness and a diffusion term that degrades roughness. When compared to acoustic data from the 1999 and 2004 Sediment Acoustics Experiments (SAX99 and SAX04), the model yields diffusivities in the range from 3.5×10^{-11} to 2.5×10^{-10} $m^2 s^{-1}$ (from 10 to 80 $cm^2 yr^{-1}$), with the larger values occurring at sites where bottom-feeding fish were active. While the experimental results lend support to the model, a more focused experimental and simulation effort is required to test several assumptions intrinsic to the model.**

***Index Terms*—Acoustic scattering, bioturbation, diffusion processes, seafloor, sediment transport.**

I. Introduction

BIOLOGICAL activity (bioturbation) at the seafloor causes small scale, random sediment transport that is often approximated as a diffusive process. In the absence of hydrodynamic forcing by storms or strong tidal currents, biological processes will dominate the evolution of bottom roughness features. As noted in [1], this was the case at one of the sites considered in this paper. The evolution of roughness has been treated as a horizontal diffusive process [2], [3]. In this view, horizontal diffusion of sediment particles due to the activity of small animals living within or near the seafloor will tend to reduce roughness features. Counteracting this degradation of roughness, biological processes also create new roughness features. If both processes act for a sufficiently long time and at constant rates, a statistical equilibrium will be reached in which details of roughness change with time while the power spectral density of random roughness is constant [1]. This assumption is used in [4] where relations between acoustic and roughness temporal correlations are developed and applied.

Manuscript received April 23, 2007; revised June 04, 2008 and January 14, 2009; accepted April 10, 2009. First published August 28, 2009; current version published November 25, 2009. This work was supported by the U.S. Office of Naval Research.

Associate Editor: J. F. Lynch.

D. R. Jackson, K. L. Williams, C. D. Jones, and D. Tang are with the Applied Physics Laboratory, University of Washington, Seattle, WA 98105 USA (e-mail: drj@apl.washington.edu; williams@apl.washington.edu; cjones@apl.washington.edu; djtang@apl. washington.edu).

M. D. Richardson and K. B. Briggs are with the Naval Research Laboratory, Stennis Space Center, MS 39529-5004 USA (e-mail: mrichardson@nrlssc.navy.mil; kbriggs@nrlssc.navy.mil).

A. P. Lyons is with the Applied Research Laboratory, Pennsylvania State University, State College, PA 16804 USA (e-mail: apl2@psu.edu).

Digital Object Identifier 10.1109/JOE.2009.2021287

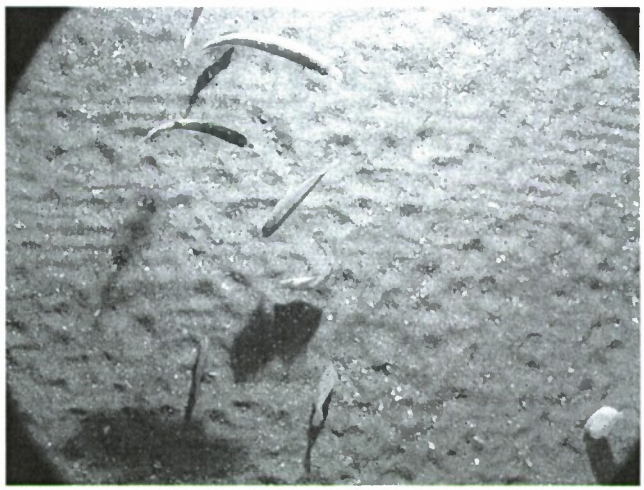

Fig. 1. Pockmarks created at the sandy SAX99 site by feeding pinfish. Note the remnant of quasi-periodic, ripple-like structure that was obliterated within 24 hours by this biological activity [6].

In this paper, similar relations are used in conjunction with a model for the time evolution of seafloor roughness [5]. This model will be examined in some detail and compared with photographic and acoustic data.

A photographic example of biological activity creating and modifying seafloor roughness is shown in Fig. 1. In the 1999 Sediment Acoustics Experiment (SAX99), conducted in shallow water in the northeastern Gulf of Mexico, fish feeding on small benthic organisms created roughness in the form of overlapping pockmarks.

Numerous studies have interpreted and quantified vertical mixing in sediments as a diffusive process, but horizontal diffusion is more relevant to the problem of roughness time evolution. Wheatcroft [3] has presented data suggesting that horizontal diffusivities are larger than vertical diffusivities by an approximate factor of ten. While most studies of sediment diffusion have focused on fine-grained clays and muds, this paper is concerned with sandy sediments. Of direct relevance to this work are measurements of horizontal diffusivity at the 2004 Sediment Acoustics Experiment (SAX04) site [2]. These measurements used high-frequency sonar images of time-varying roughness and obtained diffusivities in the range from 1 to 20×10^{-9} $m^2 s^{-1}$ (from 300 to 6000 $cm^2 yr^{-1}$). The same data set is discussed extensively in [1] although diffusivity values are not given. Applying a method developed below, a diffusivity of 3.2×10^{-9} $m^2 s^{-1}$ (1000 $cm^2 yr^{-1}$) can be obtained from the spectral decay data of [1]. In this paper,

diffusivity will be denoted D and given in SI units. The more traditional units (cm^2/yr) will also be given occasionally to facilitate comparison with the literature.

Mathematical models have been developed to describe transport of sediment particles by bioturbation. The most common are 1-D biodiffusion transport models that employ a depth-dependent biodiffusion or mixing coefficient which characterizes the intensity of vertical mixing as a function of depth [8]. Most models for biodiffusion are based on measurements of particle transport in the vertical direction, using solid-phase continuous or impulsive tracers such as naturally occurring radionuclides (Pb-210, Th-235, Cs-137, Be-7), radionuclides associated with fallout from nuclear testing (Pu-239, Pu-240), or by introduced tracers such as luminophores or labeled glass beads. Vertical mixing coefficients measured in coastal sediments typically range between 3 and 30×10^{-11} m^2s^{-1} (from 10 to 100 cm^2yr^{-1}) over characteristic depth scales of 10–30 cm [9]–[11]. This rapid mixing of surficial sediments tends to obliterate signatures of depositional layers over scales of tens of years. Measured diffusivities often decrease with depth in the sediment and can be modeled as decreasing or layer-specific mixing coefficients.

A seafloor-mounted, rotating sonar platform operating at 40 kHz was used to observe changes in seafloor backscatter at the Sediment Transport on Shelves and Slopes (STRESS) site off the northern California coast [12], [13]. The complex correlation between seafloor echoes acquired at different times (defined later in this paper and referred to as the "ping-to-ping correlation") yielded a decorrelation time on the order of one month. Decorrelation times of the same order were reported for a site off Orcas Island in Washington State [5], [14], [15]. At both the STRESS and Orcas sites, the seafloor was a soft mud, and the changes were attributed to biological activity altering the details of volume scattering within the sediment. As the present interest is in changes in seafloor roughness, measurements on harder sandy seafloors are of primary interest. For such seafloors, acoustic scattering due to roughness is expected to dominate volume scattering for grazing angles smaller than the critical angle (about 30° for the sandy sites considered here). Short-term backscatter fluctuations at two sandy sites were ascribed by Stanic and Kennedy [16], [17] to water-column fluctuations rather than changes in the seafloor. As part of the coastal benthic boundary layer (CBBL) program, longer term observations at a sandy site were carried out at 40 kHz [18]. The results were presented in terms of ping-to-ping correlation and exhibited a decorrelation time on the order of one day. Numerous shell pieces lay upon the seafloor and it is possible that these discrete scatterers played a significant role in scattering. During SAX99, similar correlation measurements were made and are reported here. Also during SAX99, the seafloor was roughened artificially and the resulting time-dependent backscattering strength was reported [6]. These data and previously unpublished data from SAX04 will be compared with the model of Jones [5].

Photographic time series are also relevant to the present subject. A series of digital stereophotographs were obtained by Lyons during SAX99 and the corresponding time-dependent roughness spectra were reported in [6]. A longer time series of digital stereophotgraphs has been obtained at a sandy site near the island of Elba, Italy [19], and at the SAX04 site [4]. In [19], changes in roughness spectra were attributed to hydrodynamic activity (forming ripples) during storms and bioturbation (mound building by mud shrimp) during quiet periods. It was suggested that the sediment mixing is primarily vertical rather than horizontal, as the mud shrimp create funnel-shaped features and mounds from U-shaped burrows while feeding. Temporal changes in backscatter strength were calculated using a model with the time-varying measured spectra as input. The changes in root mean square (RMS) roughness were found to be small compared to diurnal changes in parameters describing the shape of the power spectral density function.

Section II defines the model in two parts: the first part is the roughness evolution model of [5], and the second part gives the connection between roughness and acoustic backscattering via conventional small-roughness perturbation theory. Section II-A considers the implications of the model for the evolution of artificially created roughness, Section II-B does the same for naturally created roughness, and Section II-C examines the statistics of the forcing term in the equation for time evolution. Section III treats issues related to acoustic measurement of time-dependent backscattering, and Section IV gives brief descriptions of the acoustic measurement systems. Properties of the experimental sites relevant to model-data comparisons are discussed in Section V, and these comparisons are made in Section VI for artificially roughened seafloors and in Section VII for naturally evolving roughness. Discussion of the present status of the model and suggestions for future work are given in Section VIII.

II. Model Definition

The model of Jones [5] allows for a position-dependent diffusivity, and the forcing term is written as a superposition of elemental "shape functions" incorporating the microtopography of individual roughness-creating events. A simplified version will be defined here, with position-independent diffusivity and with the forcing term defined in rather general terms, but constrained by assumptions regarding its independence relative to the existing relief. Time-dependent seafloor roughness will be described by the function $f(\mathbf{R}, t)$ giving the vertical displacement of the seafloor from the mean horizontal plane. The variable $\mathbf{R}$ is a 2-D vector composed of the x- and y-coordinates (horizontal), $\mathbf{R} = (x, y)$. Throughout the remainder of this paper, $f(\mathbf{R}, t)$ will be referred to as the "relief function."

The model is defined by the differential equation governing the time dependence of the relief function as well as by the assumed statistical properties of the terms in this equation. Specializing an equation given in [5], the 2-D relief function will be assumed to obey

$$\frac{\partial f(\mathbf{R}, t)}{\partial t} = D\nabla^2 f(\mathbf{R}, t) + S(\mathbf{R}, t). \tag{1}$$

The first term on the right-hand side in (1), the diffusion term, causes roughness to decay with time, while the second term, the forcing term, counteracts this decay. The diffusivity D is the defining parameter of the model and is also the parameter to be estimated in fits of the model to data. As both diffusion and

forcing are assumed to be due to biological activity, it is reasonable to inquire as to which sort of activity leads to diffusion and which leads to roughness generation. No definitive answer is offered here, but Hay [1] ascribes ripple decay in his SAX04 data to bottom-feeding fish. In [14], it is suggested that diffusion results from the activity of smaller animals and mechanical collapse of features created by larger animals, while forcing represents the activity of larger animals. In the present problem, it can be asserted that the forcing term represents the creation of feeding pits and other features. The forcing term will be assumed to be statistically uncorrelated with the relief function

$$\langle f(\mathbf{R}_1, t)S(\mathbf{R}_2, t)\rangle = 0\,. \tag{2}$$

The symbols $\langle\rangle$ denote a formal average of an ensemble of different random realizations of the relief function and forcing term. It is important that both are evaluated at equal times t in (2). There will be some correlation between the forcing term at any given time and the relief at a later time, as part of this relief results from the forcing. Equations (1) and (2) embody assumptions whose primary motivation is simplicity, but which may prove to be approximately true in real situations. First, (1) says that the effect of the forcing term is simply additive. In combination, (1) and (2) require that feeding pits, etc., cannot be preferentially located with respect to features of the topography. For example, it is conceivable that feeding by fish as in Fig. 1 will take place preferentially at highs or lows of the topography, but this is not allowed by the model. Equations (1) and (2) also do not allow the shape of any feeding feature (such as a pit) to be influenced by the preexisting topography. That is, the shape of the pit (defined by the change in z-coordinate over the pit with respect to the preexisting topography) is the same whether the pit occurs at a topographic high, a topographic low, or on a slope. While it is certain that these assumptions cannot be strictly true, the issue is whether they provide useful approximations.

The final assumption is that the forcing term $S(\mathbf{R}, t)$ is a stationary random process with respect to spatial coordinates and time. That is, biological creation of roughness proceeds at a steady pace for all times of interest and has constant strength over the seafloor area of interest. While the assumption of temporal stationarity is also used in [4], those authors note that it was not well satisfied in their SAX04 data. Temporal changes in roughness spectra have also been reported in [19] and [20]. On the other hand, Hay [1] finds that roughness spectra measured during SAX04 exhibit stationarity in the high-frequency band (8–24 cycles/m, this is wave number divided by 2π). In this paper, we depart from SI practice in denoting the units of spatial frequency by either cycles per meter or radians per meter, as appropriate. A major cause of temporal nonstationarity is the diurnal behavior of animals living near or within the seafloor. For example, the diurnal changes in roughness documented in [19] were due to changes in the activity of burrowing shrimp. Fish commonly exhibit diurnal behavior, forming schools during the day and descending in the water column. Also, small animals are known to emerge from the seafloor into the water column at night [21]. If roughness statistics are observed and averaged over several days, it may be reasonable to treat animal activity as stationary on these time scales. In this paper, the stationarity assumption is made primarily on the grounds of simplicity and could be avoided by allowing the forcing term to have temporal changes in its statistics on time scales much longer than those characterizing the roughness-causing events. As these events have time scales measured in seconds or less, this approach is feasible, but not warranted at present owing to lack of information on the slow time dependence of biological activity at the experimental sites.

When artificial roughness is introduced, it will be modeled as an additive initial term in the relief function and not as a term in the forcing function. If there is no artificial modification of roughness, and if the forcing term is statistically stationary and has acted for a sufficiently long time, the spectrum of naturally created roughness will reach a time-independent equilibrium value. The relief function itself will change with time, but the resulting spectrum will be constant in time. From the point of view of the present development, this equilibrium spectrum can be considered a parameter of the model because it will be used to determine the statistics of the forcing term (actually, the spectrum provides many parameters, as it is always measured over a range of spatial frequencies).

The link to acoustic scattering is provided by small-roughness perturbation theory, which can be used to show that the complex backscattered pressure at time t is of the form

$$P = \frac{H}{r^2}e^{2ikr}F(\mathbf{K}_B, t)\,. \tag{3}$$

In this expression, H is a factor depending on the acoustic frequency, grazing angle, and acoustic parameters of the water and sediment (mass density, sound speed, and attenuation). A nondirectional, continuous-wave source is assumed with slant range r from the source to the scattering location of interest. The Fourier transform of the relief function is represented by the notation $F(\mathbf{K}, t)$, where

$$F(\mathbf{K}, t) = \frac{1}{(2\pi)^2}\int f(\mathbf{R}, t)e^{-i\mathbf{K}\cdot\mathbf{R}}d^2R \tag{4}$$

and where $\mathbf{K} = \langle K_x, K_y\rangle$ is a 2-D wave vector. In (3), the Fourier transform is evaluated at the Bragg wave vector $\mathbf{K}_B = \langle 2k\cos\theta, 0\rangle$, where $k = \omega/c$ is the acoustic wave number in water, and θ is the grazing angle. Equation (3) is derived under the assumption that the relief function falls to zero outside a small seafloor patch situated at slant range r from the source. This contradicts the earlier assumption that the relief function is a stationary random process with respect to the horizontal spatial coordinates. This contradiction can be avoided by assuming a directional source, but the formalism becomes more involved. In the present approach, one can take the relief function to be the product of a stationary process and a smooth spatial window function. If the window is wide compared to the horizontal scales of roughness of interest, yet small compared to the slant range, the assumption of spatial stationarity can still be employed.

From (3), the covariance of backscattered pressure $\langle P_2P_1^*\rangle$ obtained at times t_1 and t_2 is of the form

$$\langle P_2P_1^*\rangle = Q\,W(\mathbf{K}_B, t_1, t_2) \tag{5}$$

where Q is an inessential factor depending upon grazing angle, frequency, and acoustic properties. The cross spectrum of relief in (5) is related to the Fourier transform of the relief function as follows:

$$\langle F(\mathbf{K}_2, t_2)F^*(\mathbf{K}_1, t_1)\rangle = W(\mathbf{K}_1, t_1, t_2)\delta(\mathbf{K}_1 - \mathbf{K}_2)\ . \quad (6)$$

The presence of the Dirac delta function is only appropriate if $f(\mathbf{R}, t)$ is stationary with infinite extent in the spatial coordinates. As a result of the windowing assumed here, the delta function is actually an approximation to a sharply peaked, but finite, function. The cross spectrum is related to the covariance of the relief function as follows:

$$W(\mathbf{K}, t_1, t_2) = \frac{1}{(2\pi)^2}\int B(\mathbf{R}, t_1, t_2)e^{-i\mathbf{K}\cdot\mathbf{R}}d^2R \quad (7)$$

where $\mathbf{K} = (K_x, K_y)$ is a 2-D wave vector, and $B(\mathbf{R}, t_1, t_2)$ is the two-time covariance of the relief function

$$B(\mathbf{R}_2 - \mathbf{R}_1, t_1, t_2) = \langle f(\mathbf{R}_2, t_2)f(\mathbf{R}_1, t_1)\rangle\ . \quad (8)$$

As a result of the stationarity approximation, only the coordinate difference appears on the left-hand side of (8). The time dependence is left general to accommodate cases in which artificial roughness is introduced, causing a breakdown of temporal stationarity.

The expressions given above will be used to treat two different problems in time dependence of backscattering. In the first problem, artificial roughness is deliberately created, and the time decay of this roughness is observed as a decay in the backscattering cross section $\sigma(\theta)$, to be defined later. The scattering cross section is proportional to the equal-time spectrum obtained by setting $t_1 = t_2$ in (7). This spectrum is evaluated at the Bragg wave vector defined earlier. In the second problem, the time dependence of natural roughness is observed through change in the details of the seafloor echo in successive pings. These changes are quantified by means of the complex ping-to-ping correlation coefficient, proportional to the cross spectrum (7) with $t_1 \neq t_2$. It will be possible to discuss both of these problems, even comparing the model with measurement data, without examining the forcing term. Later, it will be shown that the assumptions embodied in (1) and (2) suffice to determine the statistical properties of the forcing term (provided the equilibrium spectrum is known). Using this idea, the forcing term will be discussed in some detail.

A. Time Decay of Artificial Roughness

During SAX99 [22], [23] and SAX04 [24], [25], artificial roughness was introduced by raking the seafloor to create regular ripple patterns that produced strong backscattering at the frequency corresponding to the Bragg wavelength [6], [25]. To address this problem without direct appeal to the forcing term, the relief function will be expressed as the sum of natural and artificial terms

$$f(\mathbf{R}, t) = f_n(\mathbf{R}, t) + f_a(\mathbf{R}, t)\ . \quad (9)$$

The artificial roughness $f_a(\mathbf{R}, t)$ is created at $t = 0$, and the natural roughness $f_n(\mathbf{R}, t)$ is assumed to evolve (even through the moment of artificial roughness creation) as it would normally. The superposition expressed in (9) is questionable for small times because the creation of artificial roughness will modify the existing natural roughness. This idealization is reasonable, however, if the artificial roughness is initially greater than the natural roughness. In this case, the time required for the artificial roughness to decay to a value comparable to the natural roughness is greater than the time required for the natural roughness to regain statistical equilibrium. In other words, by the time the artificial roughness decays to a level where it no longer masks the natural roughness, the natural roughness will have returned to equilibrium. The natural roughness is time dependent owing to the competing processes of generation and diffusion, but it has a time-independent power spectral density $W_n(\mathbf{K})$. As the natural roughness term in (9) satisfies (1), the artificial roughness must obey the diffusion equation with no forcing

$$\frac{\partial f_a(\mathbf{R}, t)}{\partial t} = D\nabla^2 f_a(\mathbf{R}, t). \quad (10)$$

It will be assumed that the two roughness components are uncorrelated

$$\langle f_n(\mathbf{R}_0 + \mathbf{R}, t_1)f_a(\mathbf{R}_0, t_2)\rangle = 0 \quad (11)$$

insuring that the overall roughness spectrum is the sum of the spectra for $f_n(\mathbf{R}, t)$ and $f_a(\mathbf{R}, t)$

$$W(\mathbf{K}, t, t) = W_n(\mathbf{K}) + W_a(\mathbf{K}, t, t)\,. \quad (12)$$

Using (6), the time-dependent spectrum $W_a(\mathbf{K}, t, t)$ can be written in terms of the Fourier transform of $f_a(\mathbf{R}, t)$

$$\langle F_a(\mathbf{K}, t)F_a{}^*(\mathbf{K}_0, t)\rangle = W_a(\mathbf{K}, t, t)\delta(\mathbf{K}-\mathbf{K}_0). \quad (13)$$

The diffusion equation (10) gives

$$F_a(\mathbf{K}, t) = F_a(\mathbf{K}, 0)\exp(-K^2Dt). \quad (14)$$

The final result for the time dependence of the roughness spectrum is

$$W(\mathbf{K}, t, t) = W_n(\mathbf{K}) + W_a(\mathbf{K}, 0, 0)\exp(-2K^2Dt) \quad (15)$$

where $W_a(\mathbf{K}, 0, 0)$ is the spectrum of the artificial roughness immediately after its creation. Note that the $1/e$ decay time is

$$T_D = \frac{1}{2K^2D}. \quad (16)$$

In practice, the time-dependent backscattered acoustic intensity is measured, but it is simply proportional to $W(\mathbf{K}, t, t)$ evaluated at the Bragg wave vector $\mathbf{K}_b$. Specializing (5) to the present case

$$\langle PP^*\rangle = QW(\mathbf{K}_b, t, t)\,. \quad (17)$$

Taken together, (15) and (17) show that the mean square backscattered pressure is the sum of a constant term due to

natural roughness and a decaying term due to artificial roughness. The initial value of the decaying term is determined by the initial artificial roughness. The backscattering cross section (which is proportional to $\langle PP^* \rangle$) is dependent on the grazing angle θ, and is defined through the relation [7]

$$\sigma(\theta) = \frac{\langle PP^* \rangle r^2}{A|P_i|^2} \tag{18}$$

where P_i is the complex amplitude of the pressure incident upon a scattering patch of area A situated at range r from the receiver at which P is measured. In the case at hand, the cross section has the form

$$\sigma(\theta) = \sigma_n(\theta) + \sigma_a(\theta) \exp(-2K_b^2 Dt) \tag{19}$$

with a constant "natural" term and a decaying "artificial" term. Equation (15) predicts that short-wavelength (large K) roughness features will decay more rapidly than long-wavelength (small K) features. Since the Bragg wave number is proportional to acoustic frequency, this leads to a prediction for the frequency dependence of the decay rate of scattering due to artificially created roughness. According to (19), the decay rate should be proportional to the square of acoustic frequency. The application of (19) to backscatter data will be discussed in Section VI.

B. Time Evolution of Natural Roughness

In the natural state, the seafloor is not disturbed by the experimentalist, and changes in the details of seafloor roughness can be observed by means of correlation between sonar echoes taken at different times. This is the ping-to-ping correlation, for which the complex cross correlation of backscattered pressure is of interest. In small-roughness perturbation theory, this correlation can be expressed in terms of the two-time cross spectrum using (5). Owing to the assumed temporal stationarity of natural roughness, the cross spectrum will only depend on the "lag," $\tau = t_2 - t_1$. The problem of measuring the pressure cross correlation will be discussed in Section III. The essential factor is the lag-dependent cross spectrum, which can be obtained from the diffusion equation by separating the relief function into a decaying part that is due to all forcing occurring for negative times and a growing part that is due to all subsequent forcing

$$f(\mathbf{R}, t) = f_d(\mathbf{R}, t) + f_g(\mathbf{R}, t). \tag{20}$$

The assumed lack of correlation between the forcing term and the relief function at any given time insures that the two components of the relief function are uncorrelated. As a result of this lack of correlation, and because $f_g(\mathbf{R}, 0) = 0$, the cross spectrum for times 0 and t can be obtained from (6) using

$$(F(\mathbf{K}_2, t)F^*(\mathbf{K}_1, 0)) = (F_d(\mathbf{K}_2, t)F_d^*(\mathbf{K}_1, 0)). \tag{21}$$

By definition, the decaying part of the roughness obeys the diffusion equation with no forcing term for $t > 0$, so $F_d(\mathbf{K}, t)$ is of the form (14). The result for the cross spectrum is

$$W(\mathbf{K}, 0, t) = W_n(\mathbf{K}) \exp(-K^2 Dt) \tag{22}$$

thus

$$\langle P_2 P_1^* \rangle = QW_n(\mathbf{K}_b) \exp[-K^2 D(t_2 - t_1)]. \tag{23}$$

Analogous to the previous result for the decay of scattering due to artificially created roughness, (23) gives a prediction for the frequency dependence of ping-to-ping correlation. Considering the two frequencies used in the experiments to be reported later, ping-to-ping correlation should decay 56 times faster at 300 kHz than at 40 kHz.

C. The Forcing Term

The forcing term $S(\mathbf{R}, t)$ in (1) represents new roughness features created near time t. Specifically, $z = S(\mathbf{R}, t)\Delta t$ is the relief of the mounds, pits, surface-penetrating tubes, etc., created in the time interval between t and $t + \Delta t$. A detailed model for the time dependence of roughness might specify the forcing term as a superposition of elemental shapes representing these features as in [5]. In this work, such details will not be considered, but the spectrum of the forcing term can be determined and may offer clues as to the nature of the forcing.

Consider the growing part $f_g(\mathbf{R}, t)$ of the relief function, defined in the previous section. Its Fourier transform obeys the differential equation

$$\frac{dF_g(\mathbf{K}, t)}{dt} = -K^2 D\, F_g(\mathbf{K}, t) + \Omega(\mathbf{K}, t) \tag{24}$$

where $\Omega(\mathbf{K}, t)$ is the spatial Fourier transform of $S(\mathbf{R}, t)$. The solution is

$$F_g(\mathbf{K}, t) = \int_0^t \Omega(\mathbf{K}, t') \exp[-K^2 D\,(t - t')]dt' \tag{25}$$

where the lower integration limit has been chosen so that $F_g(\mathbf{K}, 0) = 0$. The spectrum for the growing roughness follows as

$$W_g(\mathbf{K}, t) = \int_0^t \int_0^t W_s(\mathbf{K}, t_1, t_2) \exp[-K^2 D\,(2t - t_1 - t_2)]dt_1 dt_2. \tag{26}$$

Here, $W_s(\mathbf{K}, t_1, t_2)$ is the two-time cross spectrum for the forcing term $S(\mathbf{R}, t)$, obtained in terms of the second moment of $\Omega(\mathbf{K}, t)$ using an expression analogous to (6). Because the forcing term is stationary with respect to time, the cross spectrum depends only on $\tau = t_2 - t_1$. Changing integration variables in (26) to τ and $t' = (t_1 + t_2)/2$, the integral over t' can be performed, resulting in

$$W_g(\mathbf{K}, t) = \frac{1}{K^2 D} \cdot \int_0^t W_s(\mathbf{K}, \tau)\{\exp(-K^2 D\,\tau) - \exp[K^2 D\,(\tau - 2t)]\}d\tau. \tag{27}$$

Dividing the spectrum into decaying and growing parts representing $f_d(\mathbf{R}, t)$ and $f_g(\mathbf{R}, t)$

$$W_n(\mathbf{K}) = W_d(\mathbf{K}, t) + W_g(\mathbf{K}, t) \tag{28}$$

then

$$W_d(\mathbf{K}, t) = W_n(\mathbf{K}) \exp(-2DK^2 t) \tag{29}$$

and

$$W_g(\mathbf{K}, t) = W_n(\mathbf{K})[1 - \exp(-2DK^2 t)]. \tag{30}$$

It can be seen that the following expression for $W_s(\mathbf{K}, \tau)$ inserted in (27) yields (30):

$$W_s(\mathbf{K}, \tau) = 2K^2 D\, W_n(\mathbf{K})\delta(\tau). \tag{31}$$

In this substitution, note that the only contribution to the integral (27) comes at $\tau = 0$. To make sense of the integral of the delta function, it should be regarded as having finite width and being an even function of τ so that its integral from 0 to any finite positive τ yields 1/2.

Expression (31) is the primary result of this section. While equivalent to [5, eq. (5.91)], it has been derived from assumptions of independence and stationarity rather than from a specific model for the forcing term. This expression shows that the two-time cross spectrum of the forcing term is completely determined by the naturally occurring roughness spectrum and the diffusivity. The factor K^2 in (31) enhances the short-wavelength parts of the forcing spectrum compared to the natural spectrum. The delta function in the time lag variable shows that the forcing term has a white temporal spectrum; that is, successive values of the random forcing time series are uncorrelated. This is consistent with the statement made in the Introduction that the time scales associated with forcing are very short so that longer term nonstationarity could, in principle, be incorporated by a rather straightforward extension of the present model.

The forcing spectrum may provide insight into details of the processes that create roughness. The factor $2K^2 D\, W_n$ is the average spectrum of the features created per unit time. In other words, if one considers the squared magnitude of the 2-D Fourier transform of the relief function for each biologically created pit, mound, etc., and averages these with weighting corresponding to rate of occurrence, the result is proportional to $2K^2 D\, W_n$.

To illustrate the action of the forcing term, simulations will be used in which a random Gaussian forcing time and space series is generated so as to obey (31). Equation (24) is implemented numerically, and an inverse Fourier transform is used to obtain realizations of the growing relief function $f_g(\mathbf{R}, t)$. This provides a simulated view of the roughness that would grow naturally if the seafloor were perfectly flat at $t = 0$. The natural spectrum is assumed to have the "von Karman" form

$$W_n(\mathbf{K}) = \frac{w_2}{(K^2 + K_0^2)^{\gamma_2/2}}. \tag{32}$$

As with all spectra employed in this paper, the integral over all $\mathbf{K}$ gives the variance of the random variable represented by the spectrum. In this case, the integral gives the mean square relief

$$h^2 = \frac{2\pi\, w_2}{(\gamma_2 - 2)K_0^{\gamma_2 - 2}}. \tag{33}$$

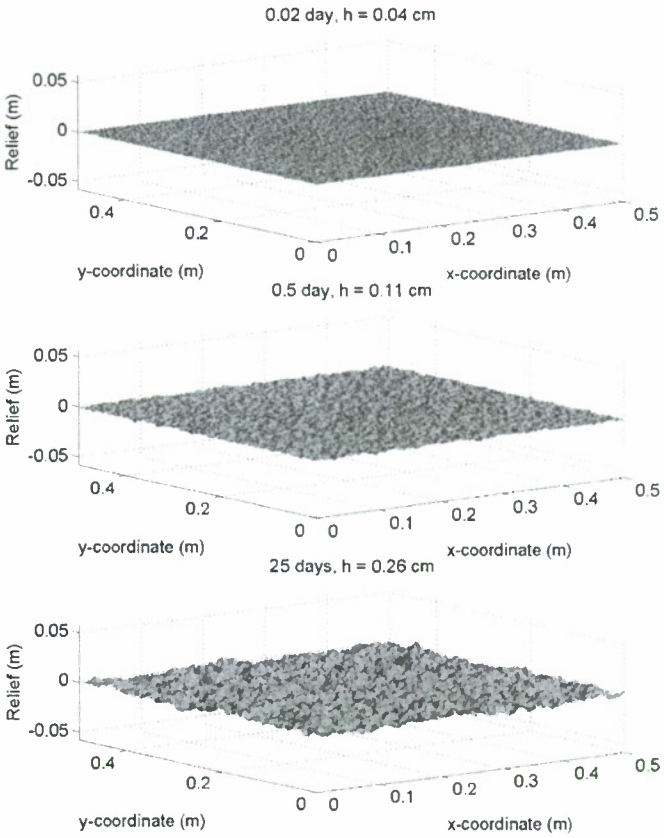

Fig. 2. Simulated growing natural relief generated using the parameters $D = 10^{-10}$ m^{2}s^{-1}, $\gamma_2 = 3.5$, $w_2 = 0.001$ m$^{0.5}$, and $K_0 = 2\pi/0.1$ m^{-1}. The interface is perfectly flat at time zero, and the growing RMS relief is denoted h.

Fig. 2 shows three selections from a simulated time series of roughness realizations generated using the method discussed in the Appendix. The last of the three realizations corresponds to a time of 25 days after the initial flat condition. After this relatively long time, roughness is near equilibrium with RMS relief 0.26 cm, to be compared with the equilibrium value 0.29 cm given by (33). Close inspection of Fig. 2 shows that the later realizations are richer in longer wavelength roughness than the earliest realization. This is seen more clearly in the corresponding spectra presented in Fig. 3, which shows that short-wavelength parts of the spectrum grow toward equilibrium rapidly while the longer wavelength parts grow more slowly. In fact, the K^2 factor in (31) suppresses the growth of large features to such an extent that the spectra exhibit a "hole" centered at the origin. This hole is evident in the theoretical spectra of the left-hand side panels but is not obvious in the spectra obtained from the roughness realizations, as the statistical uncertainty is rather large.

III. Acoustic Measurement Issues

Observation of the time dependence of backscattering strength and ping-to-ping correlation involves issues not encountered in typical backscatter measurements. Any measurement of time dependence must employ sufficient averaging to reduce the effect of statistical fluctuations to a level that will not mask the sought-after change. In some respects, however, acoustic measurements of roughness evolution are easier than

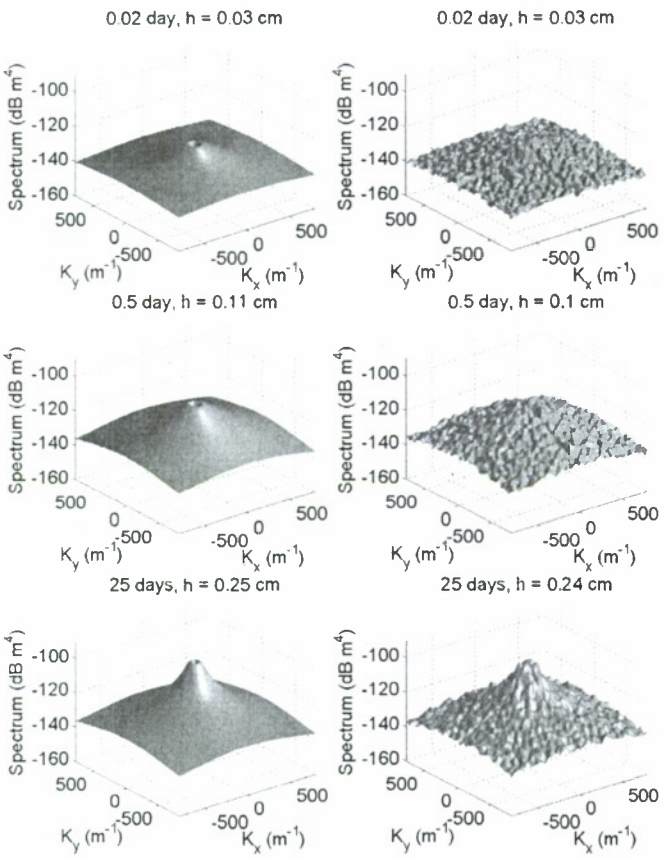

Fig. 3. The spectra of the simulated surfaces of Fig. 2 (right-hand side panels) compared with the theoretical spectra given by (30) (left-hand side panels).

conventional measurements of backscattering, which demand accurate knowledge of experimental geometry as well as transducer properties including source level, receiver sensitivity, and directivities. In contrast, the measurements to be discussed in the following sections involve comparisons of acoustic data taken at different times and do not require complete characterization of the measurement apparatus and geometry.

A measurement of backscattering strength is essentially a measurement of the mean square pressure envelope. The required averaging is usually obtained by means of successive pings taken from different patches of the seafloor. This is accomplished either by motion of the sonar over the seafloor or by pointing the sonar successively toward different portions of the seafloor. These methods are not acceptable in the present case because the changes in scattering patch location will mask changes due to biological activity. Instead, the mean square envelope can be estimated from single echoes by means of an average over a portion of the echo time series

$$\sigma_P^2 = \frac{1}{T}\int P(t)P^*(t)dt\,. \tag{34}$$

Here, $P(t)$ is the complex (baseband) pressure signal, the asterisk denotes complex conjugation, and the integral is over a time window of length T. This window is the "range gate," centered at a time corresponding to the range of interest. A notational difficulty arises at this point because two different time scales are required in this paper. The time scale used in (34) can be termed "fast time" as it is measured in milliseconds and is the round-trip acoustic time-of-flight from the sonar to the seafloor and back. This is distinct from "slow time," which is the time between any two pings that are to be compared. This slow time was used in the model development earlier and is of the order of the time required for significant changes to occur in the seafloor, hours to days. In practice, the integral in (34) will be approximated by a sum over samples taken at discrete times. If the pressure is a Gaussian random process, it can be shown that the normalized standard deviation for this estimate (standard deviation divided by the mean) can be approximated by

$$\frac{\sqrt{\left\langle \left(\sigma_P^2\right)^2\right\rangle - \left\langle \sigma_P^2\right\rangle^2}}{\left\langle \sigma_P^2\right\rangle} = \frac{1}{\sqrt{TB}} \tag{35}$$

where B is an effective bandwidth, defined as [26]

$$B = \frac{\left[\int \Phi(f)df\right]^2}{\int \Phi^2(f)df}. \tag{36}$$

In this expression, $\Phi(f)$ is the power spectrum of the transmitted waveform. Remembering that all signals are represented in baseband, the spectrum is centered at $f = 0$, and it can be seen that the effective bandwidth coincides with the width of a rectangular spectrum, as it should. The approximation leading to (35) assumes that the time-bandwidth product TB is much larger than unity. The symbols $\langle\rangle$ in (35) have the same meaning as earlier: they denote a formal ensemble average. Thus, two types of averages are of interest. Sample averages, as in (34), are applied to data and result in estimates of such quantities as mean square pressure and correlation. Formal averages give the theoretical predictions of the model and are also used in estimating the error in sample averages, as in (35). The time-bandwidth product can be interpreted as the effective number of independent samples in the windowed time series. Thus, the uncertainty in estimates such as (34) is not determined by the actual number of samples, as an increase in sampling rate results in higher correlation between adjacent samples and does not improve the estimate. In consequence, the sampling rate is not of particular importance as long as the Nyquist criterion is satisfied.

If one hopes to observe changes in scattering strength on the order of 3 dB, the normalized standard deviation must be smaller than unity. Thus, it is desirable to have large bandwidth, though not so large that the single-frequency assumption inherent in the above perturbation-theory expressions is not satisfied. The averaging window width, T sets the range resolution, and it follows that one is better off not seeking high resolution by reduction in the averaging window width. The value of $1/(TB)^{1/2}$ for the acoustic results to be reported here is about 0.27 for processing of the 40-kHz data and 0.39 for processing of the 300-kHz data.

Even for relatively "hard" sandy seafloors, backscattering is not wholly due to interface roughness; there will be a volume scattering component resulting from heterogeneity of the sediment. This situation can be accommodated in (19) by identifying $\sigma_n(\theta)$ as the natural scattering cross section resulting from both roughness and sediment heterogeneity. In short, $\sigma_n(\theta)$ is

the asymptotic value of the cross section that is observed before the artificial roughness is created and after it has decayed to zero.

Correlation estimates can be made using the following complex correlation coefficient [12], [14], [15], [27], [28]:

$$C(\tau) = \frac{\int P_2(t)P_1^*(t)dt}{\left[\int P_1(t)P_1^*(t)dt \int P_2(t)P_2^*(t)dt\right]^{1/2}} \tag{37}$$

where $P_1(t)$ and $P_2(t)$ are the complex baseband echo signals received from two different pings transmitted with time difference $\tau = t_2 - t_1$, where these are "slow times." The integral is over a (fast time) window of width T. The correlation estimate provided by (37) is an irrational function of the signals and rather difficult to analyze statistically. In order to approximate the statistical "floor" of the correlation estimate, one can consider the case of two echo signals $P_1(t)$ and $P_2(t)$ that are Gaussian and uncorrelated, with $TB \gg 1$. In this case, the approximate formal expression

$$\frac{\langle |K_{12}|^2 \rangle}{\langle \sigma_P^2 \rangle^2} = \frac{1}{TB} \tag{38}$$

can be obtained, where

$$K_{12} = \frac{1}{T}\int P_2(t)P_1{}^*(t)dt\,. \tag{39}$$

Expression (38) is not the standard deviation of the correlation estimate (for two uncorrelated signals), because the required variance would have to deal with moments of the irrational expression (37). However, if $TB \gg 1$, the relative fluctuations of the normalizing denominator of (37) will be small. If these fluctuations are neglected, (38) can be considered an approximation to the variance of the correlation estimate for the case of two uncorrelated echoes. If one hopes to estimate nonzero correlations that are substantially less than unity, the standard deviation of the estimate must be small compared to unity, that is, $1/(TB)^{1/2} \ll 1$. In the work to be reported, correlation estimates are made for each pixel in a sonar image (with range-gate width T) using the absolute value of (37). These absolute values are then averaged over many pixels to provide the final correlation estimate. Even if the echoes being compared are completely uncorrelated, the estimate will be nonzero, and this "floor" value can be approximated as follows. First, as the estimate (37) involves a sum with several terms, it will be approximated as Gaussian, with absolute value that is Rayleigh-distributed. According to (38), the mean square value of this Rayleigh random variable is approximately $1/(TB)$. It follows that the asymptotic value of the mean correlation estimate is approximately

$$\langle |C(\infty)| \rangle = \frac{1}{2}\sqrt{\frac{\pi}{TB}}\,. \tag{40}$$

Just as in the case of scattering strength estimates, it is desirable to have large bandwidth and as wide an averaging time window as permitted by range resolution requirements.

As with scattering strength estimates, correlation estimates are complicated by the fact that both roughness and volume scattering contribute to the echo signal. Because volume echoes tend to decorrelate on much longer time scales than those due to roughness scattering [18], a simple expression that can accommodate volume scattering can be obtained by a slight generalization of (23) and (37) leading to

$$C(\tau) = (1-\gamma)\exp\left(-\frac{\tau}{T_d}\right) + \gamma \tag{41}$$

where $0 < \gamma < 1$ is the asymptotic value of the correlation estimate for large lag times, and where $T_d = 2T_D$, with T_D given by (16). The nonzero value of this asymptote is due to both the presence of unchanging scattering (e.g., due to volume heterogeneity not subject to rapid change) and also due to the unavoidable variance of the correlation estimate as discussed above. Thus, the parameter γ must be larger than $\langle |C(\infty)| \rangle$ as given by (40). Expression (41) is presented as a hypothesis without proof, and the parameter γ has the burden of incorporating both unknown scattering mechanisms and the statistical "floor" of correlation estimates (40). This parameter will be determined by fits to ping-to-ping correlation data.

IV. Acoustic Measurement Systems

Two bottom-mounted, rotating sonar systems were used, the BAMS, operating at 40 kHz and the XBAMS, operating at 300 kHz. These are autonomous systems that execute circular scans according to a preset schedule. The azimuthal, 3-dB, full beamwidths were 5° for the 40-kHz system and 1° for the 300-kHz system. These beamwidths are equal to the azimuthal step made between successive pings. As the same transducer was used for transmission and reception, the round-trip beamwidths are smaller by a factor of about 0.71, and the sidelobe levels are quite low. Both systems transmitted unshaded linear frequency modulated up-sweeps having source levels of approximately 217 dB re 1 μPa and pulse lengths of 2 ms. The sweep widths were 2 and 10 kHz centered at 40 and 300 kHz, respectively. The echo data analyzed in this paper were in complex baseband form with sampling frequencies of 2 and 20 kHz. These data were matched filtered before final processing with the exception of the earliest experiment [Coastal Benthic Boundary Layer (CBBL), reported below]. Matched filtering has little effect on the 40-kHz cross-section and correlation estimates, as the window width ($T = 6.7$ ms) is large compared to the pulse length (2 ms).

Both BAMS and XBAMS employed tripod platforms. For the earlier BAMS measurements reported below (CBBL), the height of the sonar above the seafloor was 5.2 m. For the later SAX99 and SAX04 measurements, the transducer height for both BAMS and XBAMS was 3 m.

V. Measurement Sites

The data to be compared with the diffusion model come from the CBBL Panama City experiment as well as from the SAX99 and the SAX04. These data represent a small part of the total acoustic and photographic data from these experiments. All three experimental sites were located on inner shelf sands in the northeastern Gulf of Mexico in water depths of 15–29 m. The primary differences in the sediments at these three sites were in the percentage of shell fragments (percent carbonate),

presence or absence of mud lenses, and oceanographic conditions that can alter seafloor roughness. Sediment physical properties (mean grain size, porosity, and bulk density) were determined from sediment samples collected using diver cores. Sediment geoacoustic properties (sound speed and attenuation) were either measured *in situ* at 38, 40, or 58 kHz, near the 40-kHz operational frequency of BAMS, or at 400 kHz on diver-collected core samples, near the 300-kHz operational frequency of XBAMS.

During the 1993 CBBL Panama City experiment, the BAMS sonar platform was deployed at 29° 41.40′ N, 85° 40.71′ W in water depth of 29 m [18]. Acoustic scans were acquired at 20-min intervals over an 18.3-day period (August 13–31, 1993). Based on sidescan sonar imagery and surface grab samples, sediments at this site varied from highly reflective coarse sand to less reflective fine sand [29], [30]. BAMS was located in an area of high relative acoustic reflectivity, with the sediment composed of a mixture of medium to coarse sand and carbonate shell hash (carbonate percentage 27% ±12.5%). Analysis of diver-core samples collected within the acoustic field of view gave a mean sediment grain diameter of 0.48 mm (1.05 ϕ), mean porosity 41.2%, and mean bulk density of 2000 kg m^{-3}. These coarse-grain sediments had a mean sound-speed ratio of 1.132 and a mean attenuation of 33.7 dB m^{-1}, measured *in situ* at 58 kHz [30]. No strong bottom currents or storms with high significant wave heights were observed during the August 1993 deployment of BAMS, suggesting any changes in bottom roughness during the acoustic experiment were a result of biological activity.

During SAX99, BAMS was deployed approximately 150 m west of the main tending vessel at 30° 22.66′ N, 86° 38.79′ W in water depth of 18.5 m [23]. Acoustic scans were acquired at 90-min intervals from October 6 to 22, 1999 and at 30-min intervals over a 15-day period beginning October 22, 1999. Only data from the second period are considered here. During the second period, a variety of manipulative experiments were conducted within the acoustic field of view of BAMS, including placing discrete scatterers on the seafloor and creating artificial roughness by raking the seafloor [6], [22], [23], [31]. Stereophotographs which were used to measure temporal changes in roughness after raking were made near the tending vessel November 4–6, 1999. Based on backscattering from 300-kHz multibeam sonar images, the site around the BAMS tower was much more uniform than during the 1993 experiments. From analysis of diver-collected core samples, the sediments were medium sands with a mean diameter of 0.42 mm (1.27 ϕ), mean porosity of 36.6%, and mean bulk density of 2074 kg m^{-3} [22]. These sediments had a mean sound-speed ratio of 1.16 [31] and mean attenuation of 12.7 dB m^{-1}, measured *in situ* at 38 kHz [22]. The acoustic measurements reported in this paper for SAX99 were collected during periods of relative calm (October 23–24 and October 30–31) where bottom currents and significant wave heights of surface gravity waves were well below the threshold of motion for medium-sand-sized particles found on the seafloor. The bottom stereophotographs reported in Section VI were also collected during periods of relative calm with bottom currents less than 10 cm s^{-1} and significant wave heights less than 1 m. These data suggest that any changes in bottom roughness during the acoustic experiments or bottom roughness characterization were the result of biological modification of the seafloor.

Experiments were conducted during SAX04 at a site approximately 2 km north of the SAX99 experimental site in water depth of 16.5 m. BAMS was deployed on September 19, 2004 at 30° 23.284′ N, 86° 38.496′ W and continued to collect data at 1-h intervals until October 6, 2004. The deployment was about ten days after landfall of Hurricane Ivan, and the seafloor was still covered with mud, presumably derived from the backwash of lagoonal sediments. Resuspension of this mud during the 11-day acoustic deployment resulted in poor visibility, restricting diver-manipulative experiments and photography; however, the mud probably insulated the rippled sand seafloor from the effects of fish feeding. After an unsuccessful first deployment, XBAMS was redeployed on October 22, 2004 at 30° 23.213′ N, 86° 38.782′ W and collected data until October 25, 2004 at 1-h intervals. Based on sidescan imagery, the sites around both BAMS and XBAMS towers were much less uniform than during the 1993 and 1999 experiments. Areas of low backscatter (presumably mud) were interspersed with strong reflections from rippled seafloor. Sediments contained layers of sand and layers of mud derived from lagoonal sediments [33]. Near the BAMS tower, the lagoonal mud was draped over a rippled sand seafloor. The XBAMS data should not be greatly affected by mud as they were acquired after the mud layer had dissipated. The medium-sand sediments had a mean diameter of 0.36 mm (1.46 ϕ), a mean porosity of 36.6%, and a mean bulk density of 2064 kg m^{-3} [24], [34]. These sediments had a mean sound-speed ratio of 1.161 and a mean attenuation of 10 dB m^{-1}, both measured *in situ* at 40 kHz [35]. Sound-speed ratio and attenuation measured at 400 kHz from diver-core samples were 1.162 and 92 dB m^{-1}, respectively. The mud sediments that covered the rippled seafloor had a mean grain size of 10 ϕ, porosity of 80%–90% and a mean bulk density of 1150–1250 kg m^{-3}. Sound speeds measured at 400 kHz were slightly less than the overlying water.

VI. Artificial Roughness Measurements

Backscattering measurements on an artificially roughened seafloor were carried out as part of the SAX99 experiment [6]. In one set of measurements the sediment was raked to produce regular ripples of approximate wavelength 1.95 cm, a value chosen to correspond to the Bragg wavelength at 40 kHz. As will be seen, these ripples caused elevated levels of backscattering, and it is the time decay of this elevated backscattering that is of interest. Fig. 4 shows images taken from stereophotographs of the seafloor before and after raking. A steady decay of the artificial roughness is evident, but, contrary to the picture presented in the Introduction, some of this decay resulted from the activity of larger bottom-dwelling fauna such as starfish, crabs, sand dollars, and fish, of which the flounder seen in the last picture in the series is representative. Roughness degradation of this sort may not be diffusive on the small scales assumed in the present model. The roughness spectra obtained from these stereophotographs are shown in Fig. 5. Note that spatial frequency is used as the spectral variable. It is equal to the wave number used in other parts of this paper divided by

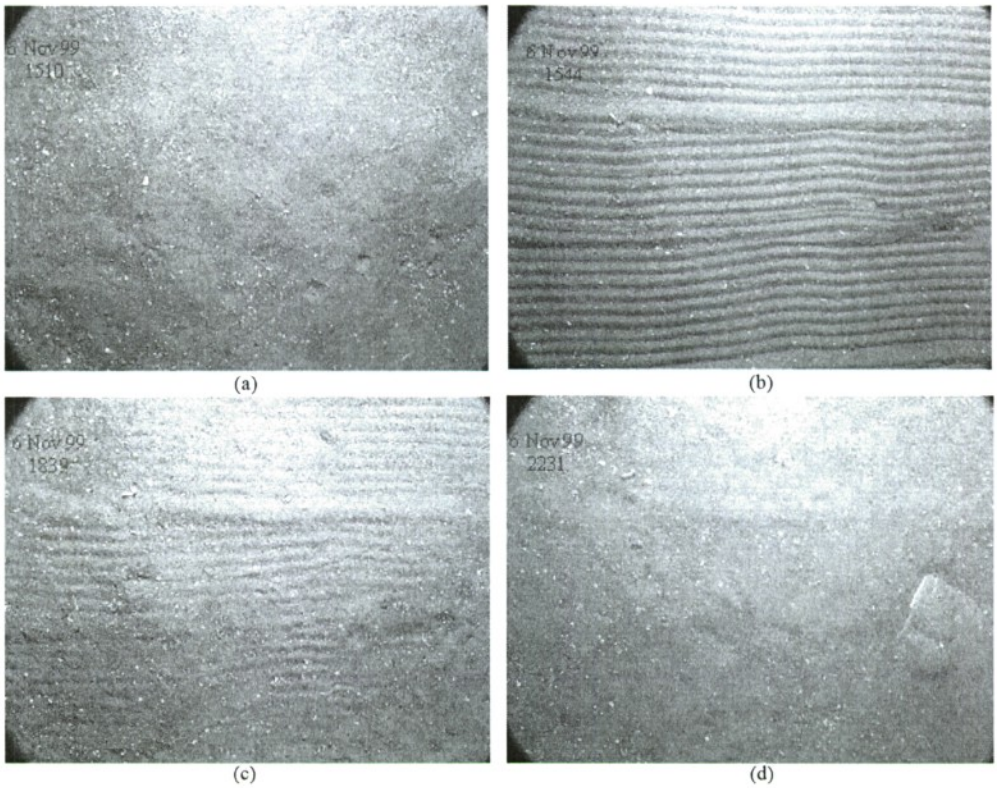

Fig. 4. Photographs taken 91 cm from the seafloor during SAX99 using a Kodak DC120 digital camera with a resolution of 1280 × 960 pixels. The photographs show the seafloor under the camera frame (a) before manipulation, (b) 6 min after raking,1.95-cm ripple wavelength, (c) 3 h after raking, and (d) 7 h after raking. A flounder, partially responsible for the decay of the artificial changes in the seafloor, can be seen in the lower right-hand side corner of the 7-h photograph. These photographs were taken during a period of calm weather. (Reproduced from [6].)

2π. Spectral peaks due to the artificial ripple are clearly visible in the spectrum immediately after raking, but these are less evident after 3 h and not seen after 7 h.

As an application of the artificial roughness model developed earlier, a value for diffusivity will be obtained from the series of spectra shown in Fig. 5. The spectrum immediately after raking will be modeled in a generalization of the form used in [6]. To insure that the spectrum has the proper symmetry, it will be broken into parts with peaks at positive and negative K_y

$$W(\mathbf{K}) = W_+(\mathbf{K}) + W_-(\mathbf{K}). \tag{42}$$

These two parts will each be divided into three subcomponents

$$W_\pm(\mathbf{K}) = \sum_{n=1}^{3} \frac{\frac{w_{2n}}{2}}{\left[a_n^2 K_x^2 + (K_y \pm K_n)^2 + \left(\frac{1}{l_n}\right)^2\right]^{\gamma_{2n}/2}}. \tag{43}$$

The parameters K_n allow introduction of spectral peaks, and the parameters a_n allow control of the anisotropy between the x- and y-directions in wave vector space. The first term in (43) will be taken to represent the natural background isotropic roughness, with the parameters K_1, a_1, l_1, w_{21}, and γ_{21} set to 0, 1, 3 cm, 0.05 cm^{-1}, and 5, to provide a rough match to the spectrum before raking. The second term in (43) represents the artificial roughness at low spatial frequencies with K_2, a_2, l_2, w_{22}, and γ_{22} set to, 0, 6, 3 cm, 0.25 cm^{-1}, and 5. The third term has K_3, a_3, l_3, w_{23}, and γ_{23} set to $2\pi/1.95$ cm^{-1}, 0.7, 7 cm, 0.05 $\text{cm}^{1.5}$, and 2.5 to match the spectral peak due to raking. To employ the model developed for decay of artificial roughness, it is only necessary to append the factor $\exp(-2K^2 D\tau)$ to the last two terms in (43), as these are the nonequilibrium terms subject to decay. The resulting time-dependent model spectrum is shown in Fig. 6 for the times given in Fig. 4. The diffusivity parameter was taken to be $D = 3 \times 10^{-9}$ m^2 s^{-1} in order to obtain an approximate match with Fig. 5. A change in the assumed diffusivity by 25% produced a clear mismatch. Fig. 6 illustrates an important feature noted earlier: high-frequency (short-wavelength) features decay more rapidly than low-frequency features. Thus, the two spectral peaks near 50 cycles/m due to raking disappear before the low-frequency lobe has returned to its natural, isotropic form.

During SAX99, backscattering measurements [6] were made using BAMS on artificial ripple fields similar to that characterized by the spectra of Fig. 5. These ripples were oriented with crest lines (equivalently, "strike") normal to the direction of the incident sound. The ripple wavelength of 1.95 cm was very close to the wavelength for Bragg scattering, 1.99 cm, which results for the frequency (40 kHz), grazing angle (15°), and water sound speed (1538 m s^{-1}) of this measurement. Scattering strength was obtained by averaging the scattering cross section over all pixels within the 2-m × 2-m raked area, with center at a horizontal range of 11 m from the BAMS rotation axis. This spatial average was then converted to scattering

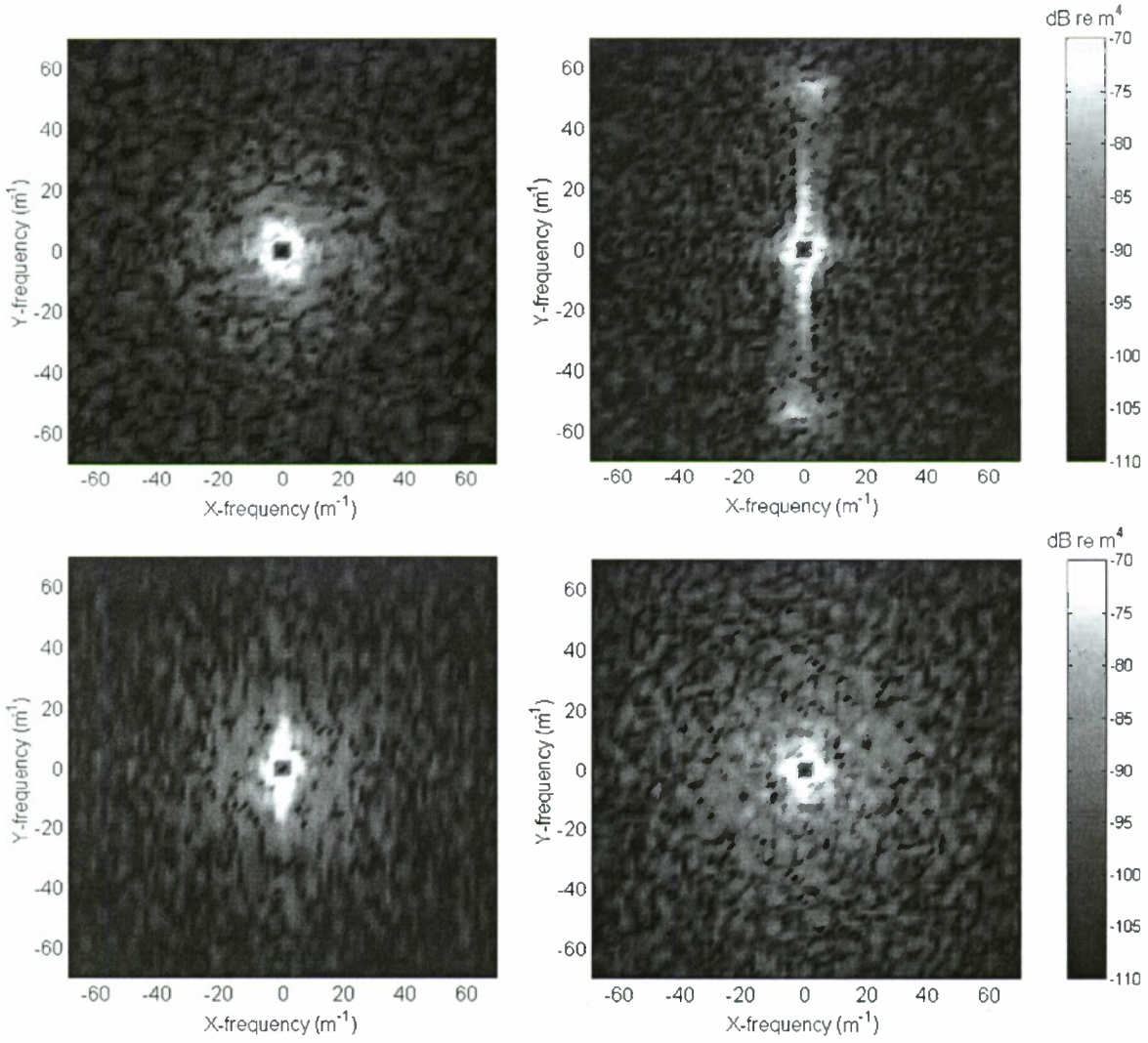

Fig. 5. Two-dimensional height spectral density levels (dB re m^4) calculated from the stereo-pair photographs corresponding to the images depicted in Fig. 4. The peaks near 50 cycles/m are due to raking of the seafloor. (Reproduced from [6].)

strength, which is equal to $10\log_{10}\sigma(\theta)$ where $\sigma(\theta)$ is the scattering cross section defined in (18). Fig. 7 shows a model fit to the results of two separate rakings, with abrupt increase in scattering strength and subsequent decay. The two rakings have differing scattering strengths, but the decay rate of both is similar. The model fit results in $D = 1.8 \times 10^{-10}$ m^2 s^{-1}. Fig. 7 shows the result of 25% changes in diffusivity, cited earlier as the uncertainty in fitting the spectra of Fig. 5. The diffusivity obtained by fitting backscattering data for SAX99 is a factor of 17 smaller than the value obtained by fitting the decaying spectrum. The difference in diffusivity values obtained from decay of the relief spectrum versus decay of backscattering accords with qualitative observations. The relief spectrum was obtained from a site near the SAX99 tending vessel, which acted as an artificial reef and attracted numerous fish (Fig. 1). The BAMS acoustic measurements were conducted a few hundred meters from the vessel where feeding fish were not so numerous. If the feeding activity accounts for roughness decay as well as roughness creation, this could explain the large difference in diffusivity seen at the two sites. This comparison makes it clear that future experiments should employ roughness and acoustic measurements that are coincident in both position and time. If the resulting diffusivities agree over a wide range of forcing conditions, this would be a partial validation of the model.

VII. Natural Roughness Measurements

Ping-to-ping correlation measurements on natural sandy seafloors were carried out during three experiments in the northeastern Gulf of Mexico, the CBBL experiment, SAX99, and SAX04. During all three experiments, measurements were made at 40 kHz using BAMS. During SAX04, measurements were also made at 300 kHz using XBAMS. Correlation estimates were made for adjacent, nonoverlapping averaging windows and for each azimuthal position in the circular scans provided by BAMS and XBAMS. Each estimate can be thought of as providing a value for a pixel in a correlation image of the seafloor near the sonar. Finally, the correlation (absolute) values were averaged over a large number of adjacent pixels, taking care to avoid inclusion of regions of obviously different scattering strength or correlation decay. The results reported here

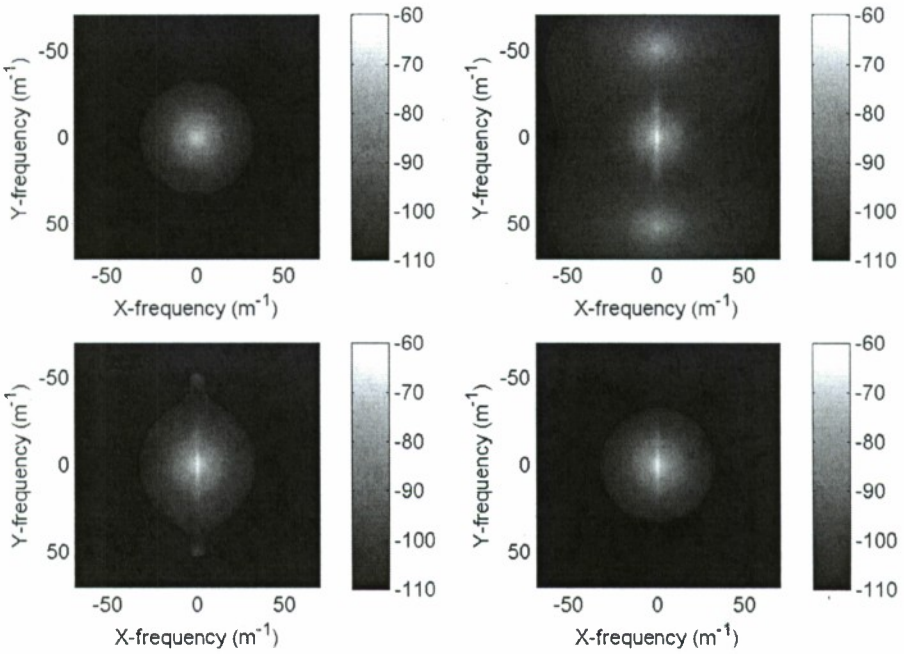

Fig. 6. Model spectra for comparison with the measured spectra of Fig. 5. The assumed diffusivity is $D = 3 \times 10^{-9}$ m^2 s^{-1}.

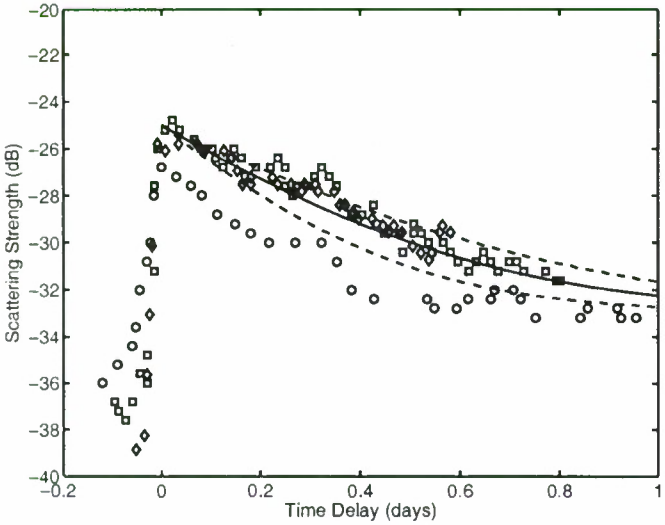

Fig. 7. Model fit to decay of scattering strength alter two different raking treatments during SAX99. The sonar frequency is 40 kHz and the nominal grazing angle is 15°. The solid curve has $D = 1.8 \times 10^{-10}$ m^2 s^{-1}, and the dashed curves correspond to diffusivities larger by a factor of 1.25 and smaller by a factor of 0.75. The initial scattering strength is assumed to be −24 dB and the asymptotic scattering strength is assumed to be −36 dB.

are merely a sampling from the available circular correlation images. For the 40-kHz measurements, the bandwidth B was 2 kHz and the averaging window width T was chosen such that $cT/2 = 5.0$ m. For the 300-kHz measurements, $B = 10$ kHz, and $cT/2 = 0.5$ m. The corresponding asymptotic correlation estimates (39) are 0.24 for BAMS and 0.34 for XBAMS. These figures represent the statistical "floor" for correlation estimates for large lag times. As noted above, the actual floor γ will be higher if slowly changing sediment volume scattering contributes to the echo signal.

Fig. 8 shows 40-kHz correlation data and model fits for CBBL and SAX04. The CBBL data were processed using the same averaging window width as for SAX99 and SAX04. The CBBL correlation estimates were averages over all 72 azimuthal steps at a horizontal range of 27.5 m. The SAX99 and SAX04 correlation estimates were averages over approximately 30 azimuthal steps centered at a horizontal range of 12.5 m. The fitted asymptotic correlation (γ) was 0.4 for CBBL and 0.45 for SAX04. These asymptotes are larger than the statistical floor of 0.24; consequently, it appears that roughly 7%–20% of the backscattered intensity must be due to sediment volume scattering that undergoes little change on time scales of several days. The SAX04 correlation curve is rather uneven owing to the intrusion of fish into the sonar field of view. This problem was even more severe for SAX99, as evident in Fig. 9. In this case, the diffusivity given in Section VI for scattering strength decay at this site provides a satisfactory fit. Fig. 10 compares measured and modeled ping-to-ping correlation at 300 kHz. These correlation estimates were averages over ten azimuthal steps and four horizontal range increments (0.5 m in size) centered at a horizontal range of 12 m. The decay rate of correlation varied substantially over the circular field of view of XBAMS, and the resulting diffusivities vary over roughly an order of magnitude, being largest near the NURC camera system, which attracted fish. The asymptotic values of the correlation estimates (0.45 and 0.5) are somewhat larger than the statistical floor (0.34), suggesting a small scattering contribution that is relatively constant with time. There is some question as to whether roughness or volume scattering dominates at 300 kHz [36]. Volume scattering presumably occurs very near the interface, as the incident grazing angle is well below the critical angle. If the interface were perfectly flat, the evanescent pressure field in the sediment would have an e-folding depth of only 2 mm. Thus, it may be that volume scattering features at such shallow depths are subject to rapid

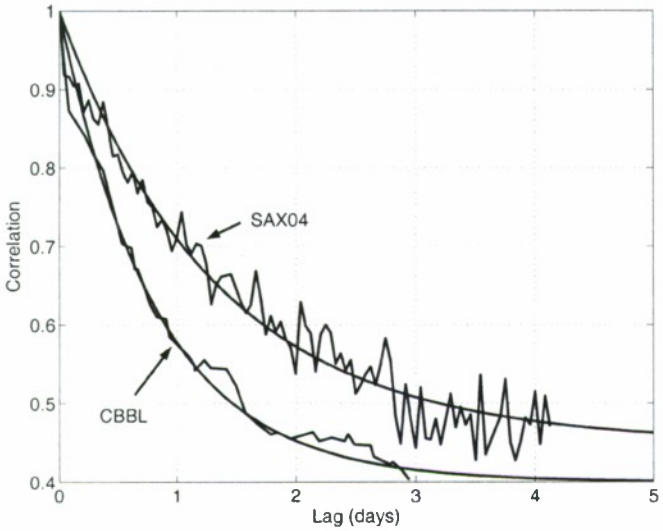

Fig. 8. Comparison of measured and modeled ping-to-ping correlation at 40 kHz for two sandy sites off the Florida Panhandle: CBBL and SAX04. The smooth curves are model results for CBBL ($D = 1.3 \times 10^{-10}$ m^2 s^{-1}, $\gamma = 0.4$, $\theta = 10.7°$) and SAX04 ($D = 9 \times 10^{-11}$ m^2 s^{-1}, $\gamma = 0.45$, $\theta = 13.5°$).

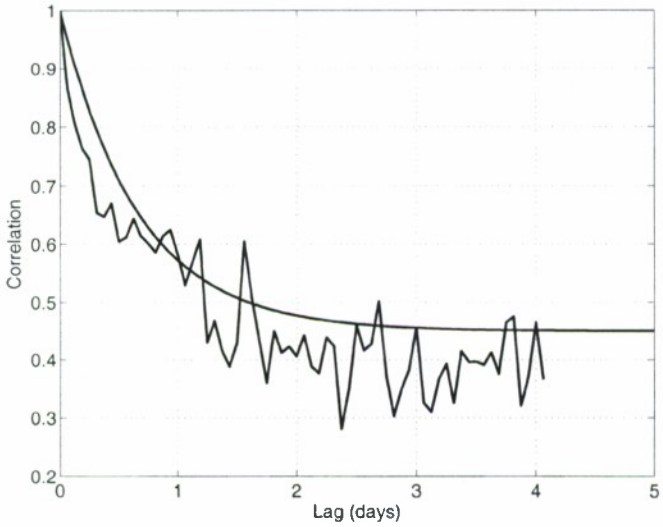

Fig. 9. Comparison of measured and modeled ping-to-ping correlation at 40 kHz for the sandy SAX99 site. The smooth curve is a model result for $D = 1.8 \times 10^{-10}$ m^2 s^{-1}, $\gamma = 0.45$, $\theta = 13.5°$.

change. Even so, it seems plausible that this change could be described as a diffusive process.

The SAX04 and SAX99 sites are in close proximity so it is reasonable to compare the diffusivities obtained in these two experiments. For SAX99, the diffusivity obtained from either backscattering decay due to artificial ripples or decorrelation of natural roughness was 1.8×10^{-10} m^2 s^{-1}. For SAX04, diffusivities are somewhat smaller, 9×10^{-11} m^2 s^{-1} at 40 kHz and about 5×10^{-11} m^2 s^{-1} at 300 kHz at locations where fish populations were relatively small. It is encouraging that the SAX04 diffusivities measured at 40 and 300 kHz are of similar magnitude even though the squared frequencies (which appear in the inversion equation) are different by a factor of 56. There is no reason to expect these diffusivities to be identical, as the

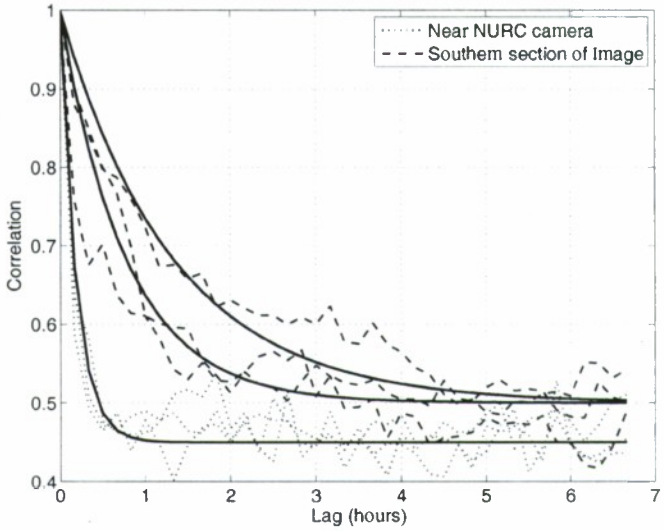

Fig. 10. Comparison of measured and modeled ping-to-ping correlation at 300 kHz for SAX04. The three smooth curves are model results for $D = 3.5 \times 10^{-11}$ m^2 s^{-1}, $\gamma = 0.5$ (upper curve); $D = 6 \times 10^{-11}$ m^2 s^{-1}, $\gamma = 0.5$ (middle curve); and $D = 2.5 \times 10^{-10}$ m^2 s^{-1}, $\gamma = 0.45$ (lower curve). All curves are computed for a grazing angle of 14°.

measurements were made at separate locations and at different times. The diffusivities measured by Hay [2] using observations of the decay of naturally generated ripples in SAX04 are larger, being in the range of $1–20 \times 10^{-9}$ m^2 s^{-1}. As noted by Hay [1], his apparatus attracted numerous fish, resulting in rapid ripple decay.

VIII. Discussion

Comparisons between diffusivities measured at different frequencies or by different methods were complicated by three factors. First, the tending vessel attracted numerous fish, so that sites near the ship had more intense biological activity than those at a greater distance. On a smaller scale, sonar and camera tripods also attracted fish, though the BAMS measurements were made at distances of order 10 m from the BAMS tripod, where fish were relatively sparse. Finally, raking the sediment exposed benthic organisms and attracted feeding fish. The least bias owing to disturbance of the natural environment should result if correlation measurements are made at ranges of tens of meters from an autonomous platform, well removed from any tending vessels.

The diffusivity values obtained in this work are reasonable, but further investigation is needed to validate or improve the model. Future experiments should include ground-truth measurement of diffusivity, e.g., by tracers, photography, or high-resolution rotary imaging sonar with short-term deployment to avoid attraction of fish. Also, multiple frequency measurements should be made at the same time to see if the estimated diffusivity is frequency independent as the model assumes. It is possible to exclude larger fauna to eliminate much of the forcing term. If the forcing term is eliminated, the diffusive term remains and roughness should decay, at least at frequencies of interest. More detailed modeling of the forcing term, as in [5], could be used to incorporate knowledge of the size and shape of feeding pits, etc. Models for volume transport such as those

of [37] and [38] could conceivably be adapted to the problem of roughness evolution and could be used to perform numerical experiments suitable for testing model assumptions such as: 1) the assumed identity between volume horizontal diffusivity and roughness diffusivity, and 2) independence of the generation and decay mechanisms.

APPENDIX

The simulation results displayed in Figs. 2 and 3 were obtained by means of a fast Fourier transform (FFT) implementation of (24). The evolving relief function is represented in the spatial frequency domain by its discrete Fourier transform $F_i(m, n)$ with the spatial frequency indices m and n ranging from 1 to N, with zero frequency corresponding to $m = n = 1$, and with spatial wave number sampling interval $\Delta K = 2\pi/L$, where the surface to be simulated has width L in both x- and y-dimensions. The time index is denoted i with time sampling interval Δt. The equation for time evolution (24) takes on the discrete form

$$F_{i+1}(m, n) = F_i(m, n)\exp(-DK_{mn}^2\Delta t) + \Omega_i(m, n)\Delta t \tag{A1}$$

with

$$\Omega_i(m, n) = a_{mn}(i)\left[\frac{2DK_{mn}^2 W_n(K_{xn}, K_{yn})}{(\Delta K^2 \Delta t)}\right]^{1/2}. \tag{A2}$$

The coefficients $a_{mn}(i)$ are complex Gaussian random variables with the conjugate symmetry required to insure that the inverse FFT of $F_i(m, n)$ is real. To produce the desired white temporal spectrum, $a_{mn}(i)$ and $a_{pq}(j)$ are independent if $i \neq j$. For the ith time step, independent, complex random numbers $b_{mn}(i)$ are generated, with the real and imaginary parts of $b_{mn}(i)$ being independent and normally distributed. The $a_{mn}(i)$ are formed from the $b_{mn}(i)$ as follows:

$$a_{mn}(i) = \frac{1}{2}[b_{mn}(i) + b^*_{(N-m+2)(N-n+2)}(i)]. \tag{A3}$$

The indexing convention in the conjugated term assumes periodicity in each index with period N. For example, setting $m = 1$, $N - m + 2 = N + 1 = 1$, modulo N. Thus, the 11 element of $a_{mn}(i)$ is equal to the real part of $b_{mn}(i)$. In the same way, one finds that, for $m = 1$ and $n > 1$, $b_{(N-m+2)(N-n+2)} = b_{1(N-n+2)}$. This says that the first row of $b_{mn}(i)$ is to be flipped in the left–right sense, with the second column replaced by the Nth, the Nth by the second, and so forth. The first column is treated analogously, and the remaining $(N-1)\times(N-1)$ matrix is flipped in both indices.

Using (A2) and (A3), and the normality and independence of the random numbers, the discrete spatial spectrum of the forcing term can be obtained from

$$\langle \Omega_i(m, n)\Omega_j^*(m', n')\rangle = 2D(K_{xm}^2 + K_{yn}^2)W_n(K_{xn}, K_{yn})\frac{\delta_{ij}}{\Delta t}\left[\frac{\delta_{mm'}\delta_{nn'}}{\Delta K^2}\right]. \tag{A4}$$

Analogous to the continuous case, the spectrum is obtained by removing the delta function factor enclosed in square brackets. The result is the discrete equivalent of (31), showing that the above prescriptions generate the correct random forcing.

The simulations of Figs. 2 and 3 employed the following parameters: $N = 256$, $L = 0.5$ m, and $\Delta t = 43.2$ s. With these choices, the highest wave number $\pi N/L$ is about 1600 rad/m with a corresponding decay time T_D of about 2000 s, showing that the chosen value of Δt allows more than adequate sampling of the decay or growth of the smallest features included in the discrete spectrum. The plots of Fig. 3 only extend to one-half the maximum wave number in order to clearly display the low-wave-number parts of the spectra. Low-frequency details are somewhat smeared by a smoothing operation used to reduce statistical noise in the right-hand side plots of Fig. 3. This filter was a 5×5 finite-impulse response filter with a Gaussian shape having response at the four corners smaller than the center response by a factor of 6. The low wave numbers of interest are of the order of the cutoff parameter $K_0 = 62.8$ rad/m. The corresponding decay time is 1.27×10^6 s. Thus, the simulation must run for more than 3×10^4 steps to follow the growth of the largest features. Fortunately, the simulation is rather efficient numerically. Unlike the split-step approximation for the parabolic equation, there is no need to perform Fourier transforms at each step. The discrete Fourier transform $F_i(m, n)$ can be marched forward in time, and the relief function in coordinate space can be obtained by a transform occasionally as desired. The diffusion propagator matrix $\exp(-DK_{mn}^2\Delta t)$ need be computed only once, as it is identical in each time step.

ACKNOWLEDGMENT

The experimental results presented here would not have been possible without the engineering and field support of R. Light and V. Miller of the Applied Physics Laboratory, University of Washington (APL-UW, Seattle). The hard work and dedication of divers of APL-UW and the Naval Research Laboratory, Stennis Space Center, MS, (NRL-SSC) was essential to the successful conduct of all three experiments, and both SAX99 and SAX04 depended on the expertise of the officers and crew of *R/V Seward Johnson*.

REFERENCES

[1] A. E. Hay, "Near-bed turbulence and relict wave-formed sand ripples: Observations from the inner shelf," *J. Geophys. Res.*, vol. 113, 2008, DOI: 10.1029/2006JC004013, C04040.

[2] A. E. Hay, "Biodegradation of wave-formed ripples during SAX04," presented at the Joint Acoust. Soc. Amer./Acoust. Soc. Jpn. Meeting, Honolulu, HI, Nov. 2006, paper 2aUW3.

[3] R. A. Wheatcroft, "Conservative tracers study of horizontal sediment mixing rates in a bathyal basin, California borderlands," *J. Mar. Res.*, vol. 49, pp. 565–588, Aug. 1991.

[4] A. L. Gerig, A. P. Lyons, E. Pouliquen, and K. L. Williams, "Comparison of seafloor roughness and scattered acoustic temporal decorrelation," *IEEE J. Ocean. Eng.*, vol. 34, no. 4, pp. 423–430, Oct. 2009, DOI: 10.1109/JOE.2008.923550.

[5] C. D. Jones, "High-frequency acoustic volume scattering from biologically active marine sediments," Ph.D. dissertation, Dept. Electr. Eng., Univ. Washington, Seattle, WA, 1999.

[6] M. D. Richardson, K. B. Briggs, K. L. Williams, A. P. Lyons, and D. R. Jackson, "Effects of changing roughness on acoustic scattering: (2) Anthropogenic changes," *Proc. Inst. Acoust.*, vol. 23, pp. 383–390, 2001.

[7] D. R. Jackson and M. D. Richardson, *High-Frequency Seafloor Acoustics*. New York: Springer-Verlag, 2007, ch. 2.

[8] N. L. Guinasso and D. R. Schink, "Quantitative estimates of biological mixing rates in abyssal sediments," *J. Geophys. Res. Oceans Atmos.*, vol. 80, pp. 3032–3043, Jul. 1975.

[9] B. P. Boudreau, "Mathematics of tracer mixing in sediments. 2. Nonlocal mixing and biological conveyor-belt phenomena," *Amer. J. Sci.*, vol. 286, pp. 199–238, Mar. 1986.

[10] R. A. Wheatcroft and D. E. Drake, "Post-depositional alteration and preservation of sedimentary event layers on continental margins, I. The role of episodic sedimentation," *Mar. Geol.*, vol. 199, pp. 123–137, Aug. 2003.

[11] J. Crusius, M. H. Bothner, and C. K. Summerfield, "Bioturbation depths, rates and processes in Massachusetts Bay sediments inferred from modeling of ^{210}Pb and $^{239+240}$Pu profiles," *Estuarine Coastal Shelf Sci.*, vol. 61, pp. 643–655, Dec. 2004.

[12] J. G. Dworski and D. R. Jackson, "Spatial and temporal variation of acoustic backscatter in the STRESS experiment," *Continental Shelf Res.*, vol. 14, pp. 1221–1238, Aug.-Sep. 1994.

[13] P. A. Jumars, D. R. Jackson, T. F. Gross, and C. Sherwood, "Acoustic remote sensing of benthic activity: A statistical approach," *Limnol. Oceanogr.*, vol. 41, pp. 1220–1241, Sep. 1996.

[14] C. D. Jones and D. R. Jackson, "Temporal fluctuation of backscattered field due to bioturbation in marine sediments," in *High Frequency Acoustics in Shallow Water*, N. G. Pace, E. Pouliquen, O. Bergem, and A. P. Lyons, Eds. La Spezia, Italy: NATO SACLANT Undersea Res. Ctr., 1997, pp. 275–282.

[15] K. L. Williams, "Temporal Fluctuations in the acoustic scattering from bottom-deployed objects and localized biological treatments," *IEEE J. Ocean. Eng.*, vol. 26, no. 1, pp. 63–69, Jan. 2001.

[16] S. Stanic and E. Kennedy, "Fluctuations of high-frequency shallow-water seafloor reverberation," *J. Acoust. Soc. Amer.*, vol. 91, pp. 1967–1973, Apr. 1992.

[17] S. Stanic and E. Kennedy, "Reverberation fluctuations from a smooth seafloor," *IEEE J. Ocean. Eng.*, vol. 18, no. 2, pp. 95–99, Apr. 1993.

[18] D. R. Jackson, K. L. Williams, and K. B. Briggs, "High-frequency observations of benthic spatial and temporal variability," *Geo-Mar. Lett.*, vol. 16, pp. 212–218, Aug. 1996.

[19] E. Pouliquen, G. Canepa, L. Pautet, and A. P. Lyons, "Temporal variability of seafloor roughness and its impact on acoustic scattering," in *Proc. 7th Eur. Conf. Underwater Acoust.*, Delft, The Netherlands, 2004, pp. 583–588.

[20] K. B. Briggs, D. Tang, and K. L. Williams, "Characterization of interface roughness of rippled sand off Fort Walton Beach, Florida," *IEEE J. Ocean. Eng.*, vol. 27, no. 3, pp. 505–514, Jul. 2002.

[21] K. Kringel, P. A. Jumars, and D. V. Holliday, "A shallow scattering layer: High-resolution acoustic analysis of nocturnal vertical migration from the seabed," *Limnol. Oceanogr.*, vol. 48, pp. 1223–1234, May 2003.

[22] M. D. Richardson, K. B. Briggs, L. D. Bibee, P. A. Jumars, W. B. Sawyer, D. B. Albert, R. H. Bennett, T. K. Berger, M. J. Buckingham, N. P. Chotiros, P. H. Dahl, N. T. Dewitt, P. Fleischer, R. Flood, C. F. Greenlaw, D. V. Holliday, M. H. Hulbert, M. P. Hutnak, P. D. Jackson, J. S. Jaffe, H. P. Johnson, D. L. Lavoie, A. P. Lyons, C. S. Martens, D. E. McGehee, K. D. Moore, T. H. Orsi, J. N. Piper, R. I. Ray, A. H. Reed, R. F. L. Self, J. L. Schmidt, S. G. Schock, F. Simonet, R. D. Stoll, D. Tang, D. E. Thistle, E. I. Thorsos, D. J. Walter, and R. A. Wheatcroft, "Overview of SAX99: Environmental considerations," *IEEE J. Ocean. Eng.*, vol. 26, no. 1, pp. 26–53, Jan. 2001.

[23] E. I. Thorsos, K. L. Williams, N. P. Chotiros, J. T. Christoff, K. W. Commander, C. F. Greenlaw, D. V. Holliday, D. R. Jackson, J. L. Lopes, D. E. McGehee, J. E. Piper, M. D. Richardson, and D. Tang, "An overview of SAX99: Acoustic measurements," *IEEE J. Ocean. Eng.*, vol. 26, no. 1, pp. 4–25, Jan. 2001.

[24] E. I. Thorsos and M. D. Richardson, "Overview of SAX04," *IEEE J. Ocean. Eng.*, 2010, to be published.

[25] M. D. Richardson, K. B. Briggs, K. L. Williams, D. Tang, D. R. Jackson, E. I. Thorsos, and P. Blondel, "The effects of seafloor roughness on acoustic scattering: Manipulative experiments," in *Boundary Influences in High Frequency, Shallow Water Acoustics*, N. G. Pace and P. Blondel, Eds. Bath, U.K.: Univ. Bath, 2005, pp. 109–116.

[26] D. R. Jackson and K. Y. Moravan, "Horizontal spatial coherence of ocean reverberation," *J. Acoust. Soc. Amer.*, vol. 75, pp. 428–436, Feb. 1984.

[27] P. A. Rona, D. R. Jackson, T. Wen, C. Jones, K. Mitsuzawa, K. G. Bemis, and J. G. Dworski, "Acoustic mapping of diffuse flow at a seafloor hydrothermal site: Monolith Vent, Juan de Fuca Ridge," *Geophys. Res. Lett.*, vol. 24, pp. 2351–2354, Oct. 1997.

[28] D. R. Jackson, K. L. Williams, T. F. Wever, C. T. Friedrichs, and L. D. Wright, "Sonar evidence for methane ebullition in Eckernfoerde Bay," *Continental Shelf Res.*, vol. 18, pp. 1893–1915, Dec. 1998.

[29] P. Fleischer, W. B. Sawyer, H. Fiedler, and I. H. Stender, "Spatial and temporal variability of a coarse-sand anomaly on a sandy inner shelf, northeastern Gulf of Mexico," *Geo-Mar. Lett.*, vol. 16, pp. 266–272, Aug. 1996.

[30] M. D. Richardson and K. B. Briggs, "In-situ and laboratory geoacoustic measurements in soft mud and hard-packed sand sediments: Implications for high-frequency acoustic propagation and scattering," *Geo-Mar. Lett.*, vol. 16, pp. 196–203, Aug. 1996.

[31] K. L. Williams, M. D. Richardson, K. B. Briggs, and D. R. Jackson, "Scattering of high-frequency acoustic energy from discrete scatterers on the seafloor: Glass spheres and shells," *Proc. Inst. Acoust.*, vol. 23, pp. 369–374, 2001.

[32] K. L. Williams, D. R. Jackson, E. I. Thorsos, D. Tang, and K. B. Briggs, "Acoustic backscattering experiments in a well characterized sand sediment: Data/model comparisons using sediment fluid and Biot models," *IEEE J. Ocean. Eng.*, vol. 27, no. 3, pp. 376–387, Jul. 2002.

[33] K. B. Briggs, A. H. Reed, D. Tang, and D. R. Jackson, "Fine-scale heterogeneity in storm-generated stratigraphy in sandy sediment of Fort Walton Beach, Florida, USA," *IEEE J. Ocean. Eng.*, 2010, to be published.

[34] M. D. Richardson, K. B. Briggs, A. H. Reed, W. C. Vaughan, M. A. Zimmer, L. D. Bibee, and R. I. Ray, "Characterization of the environment during SAX04: preliminary results," in *Proc. Underwater Acoust. Meas., Technol. Results*, J. S. Papadakis and L. Bjorno, Eds., Heraklion, Crete, 2005, pp. 285–292.

[35] M. A. Zimmer, L. D. Bibee, and M. D. Richardson, "Measurement of the frequency dependence of the sound speed and attenuation of seafloor sands from 1 to 400 kHz," *IEEE J. Ocean. Eng.*, 2010, to be published.

[36] K. L. Williams, E. I. Thorsos, D. Tang, D. R. Jackson, and K. B. Briggs, "Acoustic backscattering from a sand and a sand/mud environment: Experiments and data/model comparisons," *IEEE J. Ocean. Eng.*, vol. 34, no. 4, pp. 388–398, Oct. 2009.

[37] B. P. Boudreau, "Mathematics of tracer mixing in sediments. 3. The theory of nonlocal mixing within the sediment," *Amer. J. Sci.*, vol. 287, pp. 693–719, Sep. 1987.

[38] J. Choi, F. Francois-Caraillet, and B. P. Boudreau, "Lattice-automaton bioturbation simulator (LABS) implementation for small deposit feeders," *Comput. Geosci.*, vol. 28, pp. 213–222, Mar. 2002.

Darrell R. Jackson received the B.S., M.S., and Ph.D. degrees in electrical engineering from the University of Washington, Seattle, in 1960, 1963, and 1966, respectively. His thesis research was directed toward applications of magnetic resonance. He received the Ph.D. degree in physics from California Institute of Technology (Caltech), Pasadena, in 1977, with a dissertation on the extraction of experimental predictions from quark-gluon theory.

He worked at Boeing as a Research Engineer. He was a faculty member at the University of Massachusetts, Amherst. Since joining the Applied Physics Laboratory (APL), University of Washington, in 1976, his research has centered on underwater acoustics. Sound scattering by the seafloor has been a dominant research topic, including inversions of scattering data for sensing of benthic activity. Since retirement in 2000, he has continued his research as a Senior Fellow at APL and coauthored the book *High-Frequency Seafloor Acoustics* with M. D. Richardson (New York: Springer-Verlag, 2007).

Dr. Jackson is a Fellow and Silver Medalist of the Acoustical Society of America.

Michael D. Richardson received the B.S. degree in oceanography from the University of Washington, Seattle, in 1967, the M.S. degree in marine science from the College of William and Mary, Williamsburg, VA, in 1971, and the Ph.D. degree in oceanography from Oregon State University, Corvallis, in 1976.

He began working at the Naval Ocean Research and Development Activity, now part of the Naval Research Laboratory (NRL), Stennis Space Center, MS, in 1977. Except for a five-year assignment as Principal Scientist at NATO's SACLANTCEN, La Spezia, Italy (1995–1989), he has worked at NRL as a Research Scientist and is currently head of the Seafloor Sciences Branch in the Marine Geosciences Division. His research interests include the effects of biological and physical processes on sediment structure, behavior, and physical properties near the sediment–water interface. His current research is linked to high-frequency acoustic scattering from and propagation within the seafloor and prediction of mine burial.

Dr. Richardson is a fellow of the Acoustical Society of America, and a member of the American Geophysical Union, the European Geophysical Society, and Sigma Xi.

Kevin L. Williams received the B.S., M.S., and Ph.D. degrees in physics from Washington State University, Pullman, in 1979, 1983, and 1985, respectively.

He worked at the Naval Coastal Systems Center, Panama City, FL, from 1985 to 1988, where his primary focus was in acoustic scattering from finite bodies and propagation into ocean sediments. In 1988, he moved to the Applied Physics Laboratory, University of Washington, Seattle, where he has worked in the area of high-frequency environmental acoustics, studying propagation through ocean internal waves and arctic ice and propagation and scattering in ocean sediments. He is currently a Principal Physicist at the Applied Physics Laboratory. He is also an Associate Professor in the Oceanography Department, University of Washington.

Dr. Williams is a Fellow of the Acoustical Society of America.

Anthony P. Lyons (M'96) received the B.S. degree *(summa cum laude)* in physics from the Henderson State University, Arkadelphia, AR, in 1988 and the M.S. and Ph.D. degrees in oceanography from Texas A&M University, College Station, in 1991 and 1995, respectively.

He was a Scientist at the SACLANT Undersea Research Centre from 1995 to 2000 where he was involved in a variety of projects in the area of environmental acoustics. Currently, he is a Senior Scientist at the Applied Research Laboratory, Pennsylvania State University, State College, where he is engaged in studies of high-frequency shallow-water propagation, acoustic interaction with the seafloor, and high-resolution characterization of seafloor sediments.

Dr. Lyons was awarded, with the recommendation of the Acoustical Society of America, the Institute of Acoustics (U.K.) A.B. Wood Medal "for distinguished contributions in the underwater application of acoustics" in 2003. He is a Fellow of the Acoustical Society of America and a member of the IEEE Oceanic Engineering Society.

Christopher D. Jones received the B.S. and M.S. degrees in mechanical engineering from the University of Massachusetts, Amherst, in 1985 and 1987, respectively, and the Ph.D. degree in electrical engineering from the University of Washington, Seattle, in 1999, specializing in acoustic and electromagnetic wave propagation and scattering.

From 1987 to 1994, he was a Researcher in the Acoustics Division and the Marine GeoSciences Division of the Naval Research Laboratory, Washington, DC. He is currently a member of the Ocean Acoustics Department, Applied Physics Laboratory, University of Washington, Seattle. His present research interests include acoustic remote sensing in the ocean, wave propagation and scattering, and acoustic sensor design.

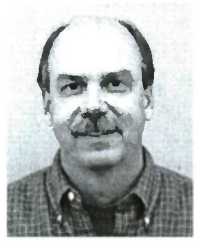

Kevin B. Briggs received the B.S. degree in biology from Florida Atlantic University, Boca Raton, in 1975, the M.S. degree in zoology from the University of Georgia, Athens, in 1978, and the Ph.D. degree in marine geology and geophysics from the Rosenstiel School of Marine and Atmospheric Science, University of Miami, Miami, FL, in 1994.

He began working at the Naval Ocean Research and Development Activity, now part of the Naval Research Laboratory (NRL), Stennis Space Center, MS, in 1979, where he was involved in research on the effects of environmental processes on sediment geoacoustic properties. He has participated in many shallow-water high-frequency acoustics experiments as an investigator of geoacoustic and roughness properties of the seafloor. He is currently engaged in research on characterization of sediment interface roughness and volume inhomogeneity for high-frequency acoustic modeling. He has over 40 published articles on physical and acoustic properties of the seafloor.

Dr. Briggs is a member of the Acoustical Society of America and the American Geophysical Union.

Dajun Tang received the B.S. degree from the University of Science and Technology, Hefei, China, in 1981, the M.S. degree from the Institute of Acoustics, Beijing, China, in 1985, and the Ph.D. degree in oceanographic engineering from the Joint Program of Massachusetts Institute of Technology and the Woods Hole Oceanographic Institution, Cambridge/Woods Hole, in 1991.

From 1991 to 1996, he was first an Assistant Scientist and then an Associate Scientists at Woods Hole Oceanographic Institution. In 1996, he moved to the Applied Physics Laboratory, University of Washington, Seattle, where he is currently a Senior Oceanographer. His research encompasses acoustics in shallow water, emphasizing impacts on acoustics by the sea bottom and water column variability.

Dr. Tang was Co-Chief Scientist for the Shallow Water 2006 (SW06) experiment.